Integrated Computational Exploring of Benzoyl Thienopyrimidine Derivatives as Potential ERa Regulators in Breast Cancer Treatment

Hassan Badaoui ¹, Marwa Alaqarbeh^{2*}, Youness Moukhliss¹, Hanane Zaki³, Moulay Ahfid El alaouy¹, M'barek Choukrad¹, Abdelouahid Sbai¹, Hamid Maghat¹, Tahar Lakhlifi¹, Mohammed Bouachrine¹

ABSTRACT

Estrogen receptor-positive (ER+) hormone-dependent breast cancer is the most common type in women, accounting for approximately 75% of all cases. This study aims to propose new potential therapeutic agents for breast cancer using computational methods. A 3D-QSAR study screened 22 compounds based on previous research, demonstrating strong predictive capabilities, as indicated by high Q² values of 0.516 and 0.787 for CoMFA and CoMSIA, respectively. Six new molecules (T1–T6) were proposed to enhance inhibitory activity, and the results of molecular docking analysis show that these drug candidates exhibit significant docking scores and form stable interactions within the receptor (PDB code: 1SJ0). The proposed compounds exhibited favorable pharmacokinetic and pharmacodynamic properties, except for T3, which showed mild toxicity. Molecular dynamics simulations also confirmed the stability of the T1–1SJ0 and 2D–1SJ0 complexes within the active site of ERα (estrogen receptor alpha). These findings highlight the potential of thienopyrimidine-based compounds as anti-breast cancer agents and open new avenues for experimental and clinical research.

Keywords: ADME/Tox, Breast cancer, Computational Modeling, 3D-QSAR, Thienopyrimidine.

1. INTRODUCTION

The broad family of nuclear receptors known as nuclear hormone receptors (NHR) functions as transcription factors. They are dispersed throughout the body and participate in cellular activities [1]. Estrone, estradiol (E2), and estriol are steroid hormones known as estrogens [2]. The most vital circulating estrogen is 17β -estradiol, which plays a crucial role in maintaining and developing reproductive organs and controlling the

activity of the immunological, circulatory, musculoskeletal, and central neurological systems. It also helps initiate and advance target tissue cancers and control energy homeostasis [3]. The estrogen receptor subtypes, ER- α and β , are crucial in mediating the physiological effects of estrogen. Estradiol binds to these receptors and activates multi-protein complexes include that coregulators. This process stimulates ER-mediated transcriptional activity through the involvement of ERa (Estrogen Receptor Alpha), AF1(Activation Function 1), and AF2 (Activation Function 2), leading to estrogenic effects [4]. The development of breast cancer occurs due to a disorder of coregulator activity, which may be

*Corresponding author: Marwa Alaqarbeh
marwaqabh@hotmail.com; marwa.aqarbeh@bau.edu.jo

Received: 17/6/2024 Accepted: 21/9/2024. DOI: https://doi.org/10.35516/jjps.v18i2.2805

¹Molecular Chemistry and Natural Substances Laboratory, Faculty of Science, Moulay Ismail University of Meknes, Morocco.

² Basic Science Department, Prince Al Hussein bin Abdullah II Academy for Civil Protection, Al-Balqa Applied University, Al-Salt, Jordan.

³ Biotechnology, Bioresources, and Bioinformatics Laboratory, Higher School of Technology, University of Sultan Moulay Sliman, Khenifra Morocco.

attributed to fluctuations in coregulator concentrations or genetic abnormalities [5]. AIB1 (Amplified in Breast Cancer 1) (ERa coregulator) increases, which induces PEA3 (Polyoma Enhancer Activator 3) mediated activation of MMP2 (matrix metalloproteinase 2) and MMP9 (Matrix Metalloproteinase 9) production, which promotes the spread of metastatic disease [6]. The process of breast cancer metastasis and invasion was facilitated by SRC-1 (Steroid Receptor Coactivator 1), an additional estrogen receptor (ER) coregulator, by its coactivation of PEA3 (Polyoma Enhancer Activator 3) mediated Twist expression. The study by Ali et al. showed that the coregulators of ERa had an impact on the modulation of gene expression in the context of metastasis [7]. Dydrogesterone is one of the essential non-acetylated pregnane derivatives and has many medical uses in treating and preventing miscarriage, supporting the luteal phase and part of menopausal treatment [8].

Heterocycle-based compounds are important in designing and developing potential drugs [9]. Pyrimidine [10], thiazole [11], quinoline [12], and imidazole [13] derivatives exhibit a variety of biological activities, among which pyrimidines are particularly important for the synthesize of antitumor drugs, including inhibitors of different cell lines [14]. Pregnanes containing imidazole rings, triazole rings, a glycoside moiety, and a piperazine ring have been demonstrated to possess anticancer and cytotoxic activity [15], antioxidant activity [16], and antileukemic properties [17], respectively. Recent studies have indicated that pyridines and pyrimidines are a category of heterocyclic nitrogen compounds with a wide

range of applications in developing anticancer drugs [18]. These synthetic sources represent a potent class of compounds that can effectively treat breast cancer. Parveen et al. have developed a novel pyrimidine conjugate (Thienopyrimidine) that exhibits specific inhibitory effects in breast cancer [19]. The antiproliferative efficacy of the synthesized conjugates was evaluated in the MCF-7 tumour cell line using the MTT assay [20].

The current study is divided into three sections. First, it uses the 3D-QSAR method to correlate the structure with the activity of a series of Benzoyl Thienopyrimidine molecules with anti-breast cancer activity. Second, it proposes new anti-breast cancer candidates with the best effect. Finally, an in-silico evaluation of the proposed molecule's ADME/Tox properties, molecular docking, and molecular dynamics predicted their stability in the target receptor. The ultimate objective is to forecast novel agents exhibiting activity surpassing that of the most potent compound within this series.

2. MATERIALS AND METHODS

2.1. Data sets

The dataset contains 22 anti-tubulin agent compounds synthesized by El-Sharkawy et al. [21]. Two arbitrary subsets were selected from this collection; one subset comprising 80% of the compounds was used for constructing the 3D QSAR model, while the other subset comprising 20% was used for model validation. The compounds' IC_{50} (μM) activity was expressed as pIC_{50} = $-\log IC_{50}$ (Table 1).

Table 1.	Chemical s	structures and	d related	activities o	of the com	ıpounds of	the studied set.

N°	1. Chemical structures and related activities of the	X		
	Molecules S N	CN X	R	Y
1a	S N	CN	-	ı
1b	\ <u>\</u>	COOEt	-	-
	X			
	, ''H ^			
	H			
2a	S N S	NH	Ph	-
2b		NH	COPh	-
2c 2d	N R	0	Ph COPh	-
20			COIII	-
	` ` ` ` ` ` ` ` ` ` ` ` ` ` ` ` ` ` `			
	H			
6a	g N	CN	-	-
6b	() N	COOEt	-	-
	0			
) H X			
	H			
8a		CN	-	-
8b		COOEt	_	_
	s N O			
	0 0			
	X			
	H			
7a	S N O	CN	-	-
7b		COOEt	-	-
	— Н X			
	H			

N°	Molecules	X	R	Y
9a	N \s	CN	-	-
9b		COOEt	-	-
	s N			
	Ö			
	\			
	н			
	H			
10a	X_	CN	-	Н
10b		CN	-	CH ₃
10c	s N	COOEt	-	Н
10d	N N	COOEt	-	CH ₃
	`х `x			
	H			
12a	N. A	CN	_	_
12b	SNNN	COOEt	_	_
120	N-0	COOL	_	_
	X			
	н			
	H			
14a		CN	-	=
14b		COOEt	-	
	N			
	s N			
	Н			
	H			

2.2. Minimization and molecular alignment

Molecular alignment is an essential stage in generating the best models of 3D-QSAR [22]. To model and optimize the chemical compounds in the studied set, a program Sybyl X-2.0 was utilized. The geometry of the compounds has been optimized using the field of Tripos forces in 1000

iterations[23]. Using the Gasteiger-Hückel concept, partial atomic loads have been computed with converge to 0.01 kcal/mol Å energy value [24]. As a result, the 2d compound, which is the most active in the compound set, is selected as a model. Other compounds have been aligned with their common maximal sub-structures (Figure 1).

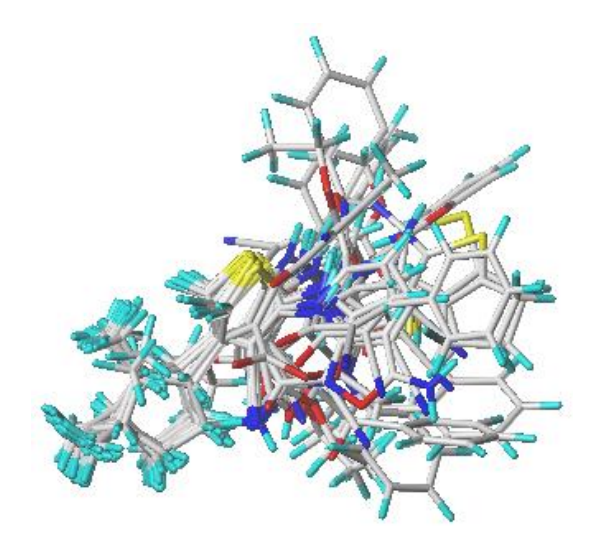


Fig. 1. Aligned compounds.

2.3. 3D QSAR studies

This study describes using the CoMFA and CoMSIA are abbreviations for Comparative Molecular Field Analysis and Comparative Molecular Similarity Indices Analysis, respectively techniques for 3D-QSAR modeling with the aid of the SYBYL-X 2.0 software[25]. Within the framework of the CoMFA modeling, a hybridized sp³ carbon atoms with a 1.52 van der Waals radius was chosen to calculate the steric and electrostatic fields, with an energy coupling of 30 kcal/mol. The same grille was used by the CoMSIA model, allowing for the calculation of additional fields, including hydrophobicity, hydrogen bond donor and acceptor, and steric and electrostatic fields. These approaches provide an investigation of molecular properties, making them invaluable in developing and discovering pharmaceuticals.

2.4. Verification of the predictive capacity of the developed CoMFA and CoMSIA models

The model generated by the method of least squares partials (PLS) was internally validated using the coefficients of cross-validation square (Q²), the number optimum de composants (ONC), the coefficient of cross-validation square (R²), and the standard error estimation (SEE). These coefficients provide a gauge of the model's

internal quality. The related expressions define Q² and R².

$$Q^{2} = \frac{\sum (y_{i} - \hat{y}_{i})^{2}}{\sum (y_{i} - \overline{y}_{i})^{2}} > 0.5$$
 (1)

$$R^{2} = \frac{\left[\sum (y_{i} - \overline{y}_{i})(\hat{y}_{i} - \overline{\hat{y}}_{i})\right]^{2}}{\sum (y_{i} - \overline{y}_{i})^{2} \cdot \sum \hat{y}_{i} - \overline{\hat{y}}_{i}} > 0.6$$
(2)

 y_i = experimental activity, \hat{y}_i = calculated activity, \overline{y}_i = = average of experimental activity, and $\overline{\hat{y}}_i$ = average of calculated activity.

2.5. The prediction of ADME/Tox and bioavailability2.5.1. Rules of Lipinski and Veber

SwissADME was used to calculate the similarity descriptors to the chosen medications using the Lipinski and Veber rules [26]. Lipinski's Rule of 5 guarantees a compound's applicability as an oral medication. A composition must meet at least two of the following requirements: molecules with PM < 500 Dalton, strong lipophilicity (LogP < 5), hydrogen bond donors (HBD < 5), and hydrogen bond acceptors (HBA < 10) [27]. Veber and colleagues have added two more relevant descriptors that are used to assess a compound's medicinal power: the number of rotative liaisons (NBR₁₀) and the surface polarity (PSA < 140 Å). The water solubility, lipophilicity,

and human intestinal absorption percentage (HIA) parameters have been used to predict absorption (LogS \leq -10: insoluble; -10 < LogS \leq -6). a little bit soluble; -6 < LogS \leq -4: moderately soluble; -4 < LogS \leq -2: soluble; -2 < LogS < 0: extremely soluble; 0 < LogS: highly soluble) [28].

2.5.2. Calculation of the ADME/Tox profile

The ADME/Tox (Absorption, Distribution, Metabolism, Elimination, and Toxicity) profile describes the chemical impact of drug candidates on health. It is a tool for predicting drug candidates' pharmacological and toxicological properties, avoiding costly late-stage preclinical and clinical failures in the preclinical phases [29].

2.6. Molecular docking

The expression of estrogen receptors characterizes MCF-7 cell lines targeted during the antiproliferative activity. The structure of the human estrogen receptor alpha domain (ERα) binding to the proposed selected 22 compounds is a target to be studied by molecular docking. Using the Auto Dock Vina program to predict the optimized binding conformation of the proposed selected 22 compounds (ligands) and understand receptor-ligand interactions [30]. After the compounds were drawn using SYBYL X2.0 software, molecular docking was carried out using Auto Dock Vina software[31].

2.6.1. Macromolecule Preparation

The RCSB database was used to retrieve the crystal structure of the human estrogen receptor alpha ligand-binding domain (ER α) in association with the antagonist (ligand 4-D) (PDB code: 1SJ0) [32]. The Discovery Studio 2016 program was used to remove the crystallized coligand, add polar hydrogens, and remove water molecules in the estrogen receptor (ER α).

2.6.2. Ligands Preparation

The most active compound in the database (2d) and the newly designed molecules (T1, T2, T3, T4, T5, and T6) were docked into the human estrogen receptor alpha (ER) [33]. The binding mode between the receptor and the

docked molecules was studied, compared, and selected for further analysis.

2.7. Molecular dynamics simulations

Molecular dynamics (MD) computations were used to determine the ideal docking positions to comprehend the stability of the interaction between a (1SJ0) protein and (T1 and D2) ligands complexes [34]. The input files for the MD calculations were generated using the CHARMM force field parameters[35]. The CHARMM force field was utilized to build the ligand topology through the Param-Chem server. The five steps of the CHARMM GUI solution builder included solving the combination and reading the coordinates of the 1SJ0) protein and (T1 and D2) ligands complex.

The experiments took place within a triclinic container filled with TIP3P water models and balanced by the addition of Na⁺ and Cl⁻ ions. Subsequently, the system underwent minimization utilizing the steepest descent technique. Following the energy minimization, the system was subjected to an NVT ensemble at 300 K for 100 ps, utilizing a v-rescale thermostat [36]. This was succeeded by an NPT ensemble at 300 K and 1 atm for 100 ps, employing a Parrinello-Rahman barostat [37] and a v-rescale thermostat [37]. Lastly, the production simulation was run at 300 K for 300 ns. The particle mesh Ewald algorithm [38] was used to figure out the electrostatic interactions, and the Linear Constraint Solver algorithm [36] was used to limit the covalent bonds.

2.7.1 Analysis of the Trajectory

Using GROMACS tools, the analysis of molecular dynamics simulations was carried out. The gmx_rms subroutine was used to calculate the ligand and the protein's root mean square deviations (RMSD) of the atom positions. Using gmx_rmsf, the quadrature-averaged fluctuations (RMSF) based on the protein's C-alpha atoms were calculated. Gmx_gyrate was used to calculate each protein's gyration radius, and Gmx_hbond was used to assess the number of hydrogen bonds at the protein-ligand interface. Also, the simulation has tracked the distance

between the protein's and the ligand's centers of mass thanks to the gmx_distance function. Finally, the trajectory visualization and frequency analysis of protein-ligand connections were conducted using the VMD 1.9.3 program [39].

2.7.2 MM/PBSA calculation of free energy of binding

A GROMACS tool called g_mmpbsa was used to perform MM/PBSA (Molecular Mechanics/Poisson-Boltzmann Surface Area) calculations for the systems chosen for additional research[40]. The free energy of binding between the (1SJ0) protein and (T1 and D2) ligands complexes in the solvent may be represented as follows:

$$\Delta G_{binding} = \Delta G_{complex} - (\Delta G_{protein} + \Delta G_{ligand})$$

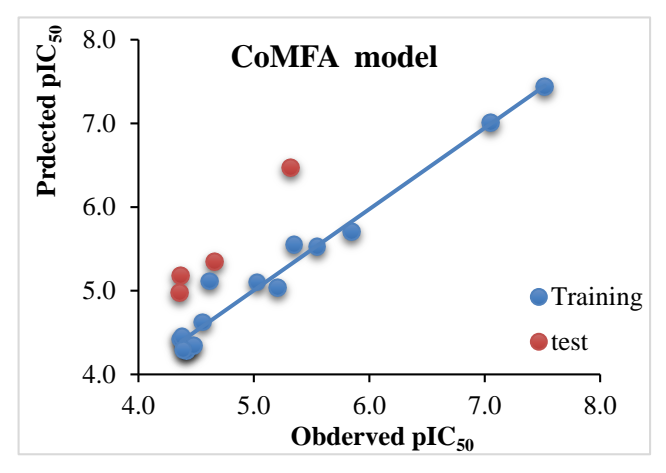
To estimate the binding energy between a protein and

ligand in a solvent, we use the isolated protein and ligand's total free energies and the protein-ligand complex's total free energies. An alternative method is to use g_mmpbsa to estimate the energy contribution of each residue to the binding energy. The binding energy can then be broken down by adding up the energy contribution of each residue. To compute g_mmpbsa's MM-PBSA, we need a binary run input file (.tpr) that reads files from specific versions of GROMACS. This file is created by GROMACS 5.1.4 [41].

3. RESULTS AND DISCUSSION

3.1. CoMFA and CoMSIA statistical findings

The real pIC_{50} about the calculated pIC_{50} for the CoMSIA and CoMFA models was illustrated in Fig. 2. The proximity of the red and blue dots creates a linear link between the observed and expected activity.



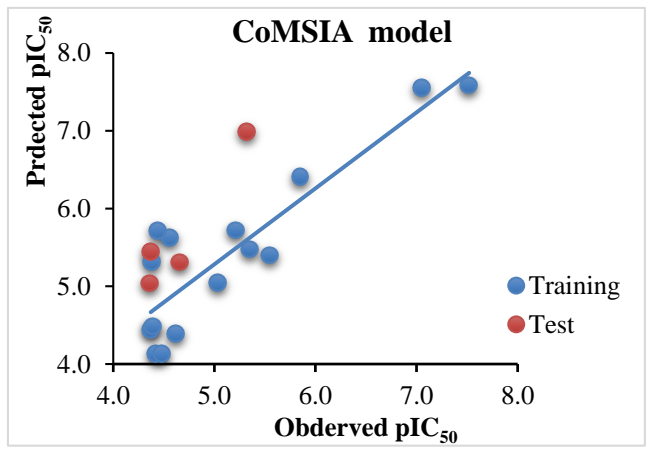


Fig. 2. Variation of the experimental activity versus the activity predicted by the CoMFA and CoMSIA models.

Tables 2 and 3 provide descriptions of the outcomes of the CoMFA and CoMSIA model validation. The outcomes satisfy all the criteria listed above.

Table 2. PLS statistical parameters.

								I	Fraction	S	
Model	Q2	R2	SEE	F	N	R ext ²	Ster	Elect	Acc	Don	Hyd
CoMFA	0.516	0.970	0.194	118.276	3	0.972	0.480	0.520	-	-	-
CoMSIA	0.787	0.993	0.093	524.592	3	0.895	0.083	0.230	0.191	0.311	0.185

Table 3. Experimental and predicted pIC_{50} of 19 thiophene, pyrimidine, pyrazole, pyridine, coumarin and isoxazole derivatives

		CoMFA		CoMSIA		
N°	pIC ₅₀	Predicted	Residual	Predicted	Residual	
10a	5.85	5.703	0.147	6.407	-0.557	
10c	5.55	5.522	0.028	5.398	0.152	
10d	5.35	5.552	-0.202	5.477	-0.127	
12a	4.62	5.111	-0.491	4.391	0.229	
12b	4.37	4.419	-0.049	4.445	-0.075	
2c	7.05	7.009	0.041	7.552	-0.502	
2d	7.52	7.437	0.083	7.583	-0.063	
6a	5.21	5.038	0.172	5.72	-0.51	
6b	5.03	5.100	-0.07	5.046	-0.016	
7a	4.42	4.28	0.14	4.130	0.29	
7b	4.38	4.447	-0.067	5.320	-0.94	
8a	4.56	4.624	-0.064	5.624	-1.064	
8b	4.44	4.339	0.101	5.713	-1.273	
9a	4.48	4.345	0.135	4.129	0.351	
9b	4.39	4.293	0.097	4.486	-0.096	
1a*	4.66	5.347	-0.687	5.309	-0.649	
14a*	4.37	5.178	-0.808	5.444	-1.074	
14b*	4.36	4.971	-0.611	5.037	-0.677	
2b*	5.32	6.472	-1.152	6.983	-1.663	

^{*} Molecule set test

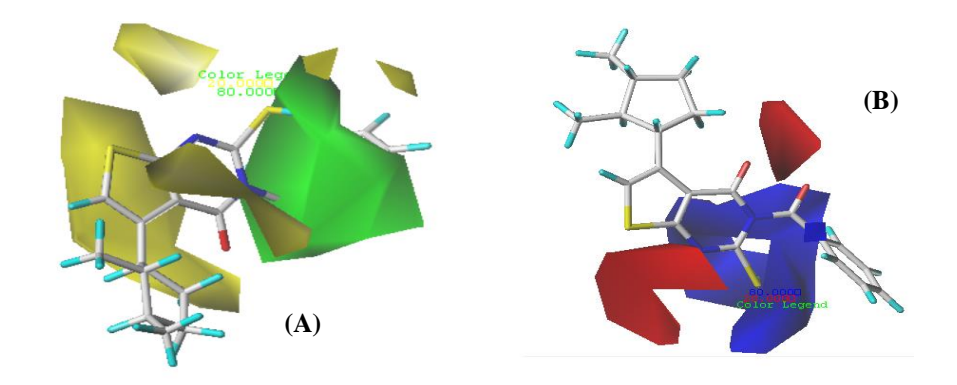


Fig. 3. (A) Steric field: yellow areas are sterically unfavorable, while green is sterically favorable. (B) Electrostatic field: blue indicates the zone where electropositive groups are favored, while red corresponds to the zone where negative groups are favored

3.2. Analysis of the results of the contour maps generated by the CoMFA model

Contextual data from contour maps is used to improve small molecule activity. On the contour maps, the most active chemical, 2d, was noted as a point of reference for interpretation.

Figure 3(A) illustrates electrostatic interactions using red and blue contours, whereas Figure 3(B) shows steric interactions of CoMFA using green and yellow contours. The green regions indicate a preference for bulky substituents, while the yellow regions indicate a preference against them. The blue sections show that nucleophilic groups are favored, while the red parts indicate that aromatization is not occurring. A) Steric specializations: the vellow outlines (20% contribution) indicate areas requiring large clusters to decrease activity, while the green contours (80% contribution) indicate regions requiring large clusters to boost activity. B) Regarding electrostatic fields, the blue contours (80% contribution) represent areas where positive charge clusters are more active. In comparison, the red contours (20% contribution) indicate areas where negative charge clusters are more active.

3.3. Analysis of the results of the contour maps generated by the CoMSIA model.

The CoMSIA analysis generated contour maps with a 2 Å grid spacing combined with compound 2D steric fields. The yellow contours (20% contribution) indicate areas where large groups are less active, while green contours (80% contribution) indicate areas of increased activity. Similarly, red contours (20% contribution) indicate areas in the electrostatic fields where electronwithdrawing groups are more active, and blue contours (80% contribution) indicate areas where they are less active. Fields with undesirable hydrophobic groups are characterized by white outlines that exhibit water-repelling properties (20% contribution), while hydrophobic groups are favored according to vellow contours (80% contribution). Magenta contours (80% contribution) indicate areas in H-bond acceptor fields where an H-bond acceptor substituent increases activity. On the other hand, red contours (20% contribution) indicate areas where an H-bond acceptor substituent decreases activity. Blue outlines (80% contribution) represent areas where the activities of the H-bond donor group increase, while purple outlines (20% contribution) indicate areas where H-bond

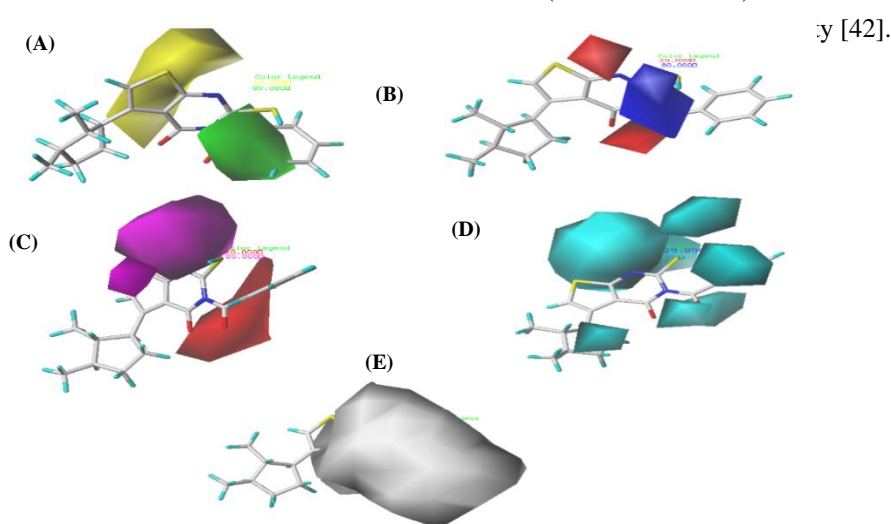


Fig. 4. 2d compound. A) Steric fields; B) Electrostatic fields.; C) H-bond acceptor fields; D) H-bond donor fields; E) Hydrophobic fields.

3.4. Drug Candidates and activity prediction

Finally, six medication candidates were recommended utilizing the field contour analysis results from the CoMFA and CoMSIA models. Table 3 illustrates the new

candidates' organization and anticipated activities, and Table 4 illustrates the new candidates' structure and predicted activities.

Table 4. Newly designed drug candidates and their predicted activities.

Table 4. Newly designed drug candidates and their predicted activities. Compound	pIC ₅₀
H ₃ C _M , H ₄ C CH ₅ CH ₅ CH ₅ T1	7.655
T2 H ₃ C CH ₃ CH ₃ CH ₃ CH ₃ CH ₃ CH ₃	7.634
T3 H ₃ C/III, H ₄ C/H ₃ CH ₃	7.618
H _b C _{M₁} H _b C H _b	7.663
T5	7.591
T6	7.549

3.4.1. The prediction of ADME/Tox and bioavailability

3.4.1.1. Rules of Lipinski and Veber

Using Lipinski and Veber's rules, the similarity

descriptors to the selected drugs were calculated with SwissADME (Table 5). Based on the results, the proposed drug candidates may be Lipinski drugs.

Table 5. ADME properties of newly designed compounds

		Property								
Rule	LogP<5	HBD<5	HBA<10	TPSA	Nrotb<10	MW ≤500				
2d compound	4,58	1	6	119	2	384.526				
T1	5.00	0	2	101.93	5	482.74				
T2	4.64	0	2	101.93	6	496.77				
T3	4.41	0	5	101.93	5	494.64				
T4	4.47	0	2	101.93	5	544.00				
T5	4.81	0	2	101.93	6	466.70				
T6	5.14	1	5	101.93	4	480.73				

3.4.1.2. Calculation of the ADME/Tox profile

The LogS values for our compounds ranged from - 5.115 to -6.494, indicating that the compounds are highly soluble (Table 6).

The percentages of the proposed drug candidates absorbed from the human gut (% HIA) were predicted using pkCSM pharmacokinetics ranging from 86.129 to 91.511% (Table 6), indicating good absorption of the compounds studied.

Blood-brain barrier (BBB) permeability is a crucial factor in pharmacological control because it helps to limit molecular transport and diffusion via the BBB while still exerting therapeutic effects on the brain [43]. The validated blood-brain barrier (BBB) permeability value in the standard scale is higher than 0.3, while a number lower than -1 is unacceptable [44]. According to the BBB assessment, all chemicals proposed under study had average BBB permeability.

P-gp in various human tissues acts as an ATP-dependent drug extraction pump, as all the proposed drug candidates are not P-gp substrates.

CYP enzyme inhibition is an essential mechanism of drug interactions based on metabolism, which exerts

another drug on the same enzymatic active site. Inhibiting CYP reduces toxicity or reduces medication effectiveness [45]. CYP2C9 is the main enzyme that metabolizes drugs [46]. It has a highly rearranged polymorphic structure, and how it is broken down differs for each person. Indeed, people with low CYP2D6 activity may not benefit as much from the drug or have harmful side effects. All proposed compounds, except T2, inhibit CYP2C9. As shown in Table 6, the compounds studied are not CYP2C19, CYP3A4, and CYP2D6 inhibitors, while they inhibit CYP1A2 [47].

Excretion is an effective method by which drugs are eliminated from the body. It is essential to determine dosing rates to achieve steady-state concentrations [48]. This descriptor's value varies between -0.361 and -0.158 ml/min/kg for the studied compounds.

AMES toxicity evaluates the potential carcinogenic effects of chemicals. When these mutant bacterial cells are exposed to mutagenic substances, the mutation in the bacterial cells is reversed, allowing the bacteria to thrive on a medium deficient in histidine [49]. T3 is the only compound that shows toxicity.

Table 6. Pharmacokinetic properties (ADMET) of new compounds.

Table of Intrinacommente properties (IDI/IDI) of new compounts.									
Models	Compounds								
Wiodels	T1	T2	T3	T4	T5		T6	2d	
Absorption									
Water solubility	-5.228	-5.214	-6.494	-6.292	-6.077		-6.081	-5.115	
Intestinal absorption (human) %	90.646	90.071	88.258	86.129	90.176	5	89.123	91.511	
P-glycoprotein substrate	No	No	No	No	No		No	No	
Distribution									
The blood-brain barrier (LogBB)	-0.065	-0.104	0.166	0.14	0.087	0.13	1	0.484	
Metabolism									
CYP1A2	No	No	No	No	No	No)	Yes	
CYP2C9	Yes	No	Yes	Yes	Yes	Ye	es	Yes	
CYP2D6	Yes	Yes	Yes	Yes	Yes	Ye	es	Yes	
CYP2C19	No	No	No	No	No	No)	No	
CYP3A4	No	No	No	No	No No)	Yes	
Excretion									
Total Clearance (ml/min/kg)	-0.308	-0.361	-0.158	-0.320	-0.266	-	0.336	-0.279	
Toxicity						•			
AMES toxicity	No	No	Yes	No	No	1	No	No	

3.5. Docking results

Table 7 and Figure 5 show the interactions between the studied compounds and the target receptor and the corresponding free energy. According to the results, all the

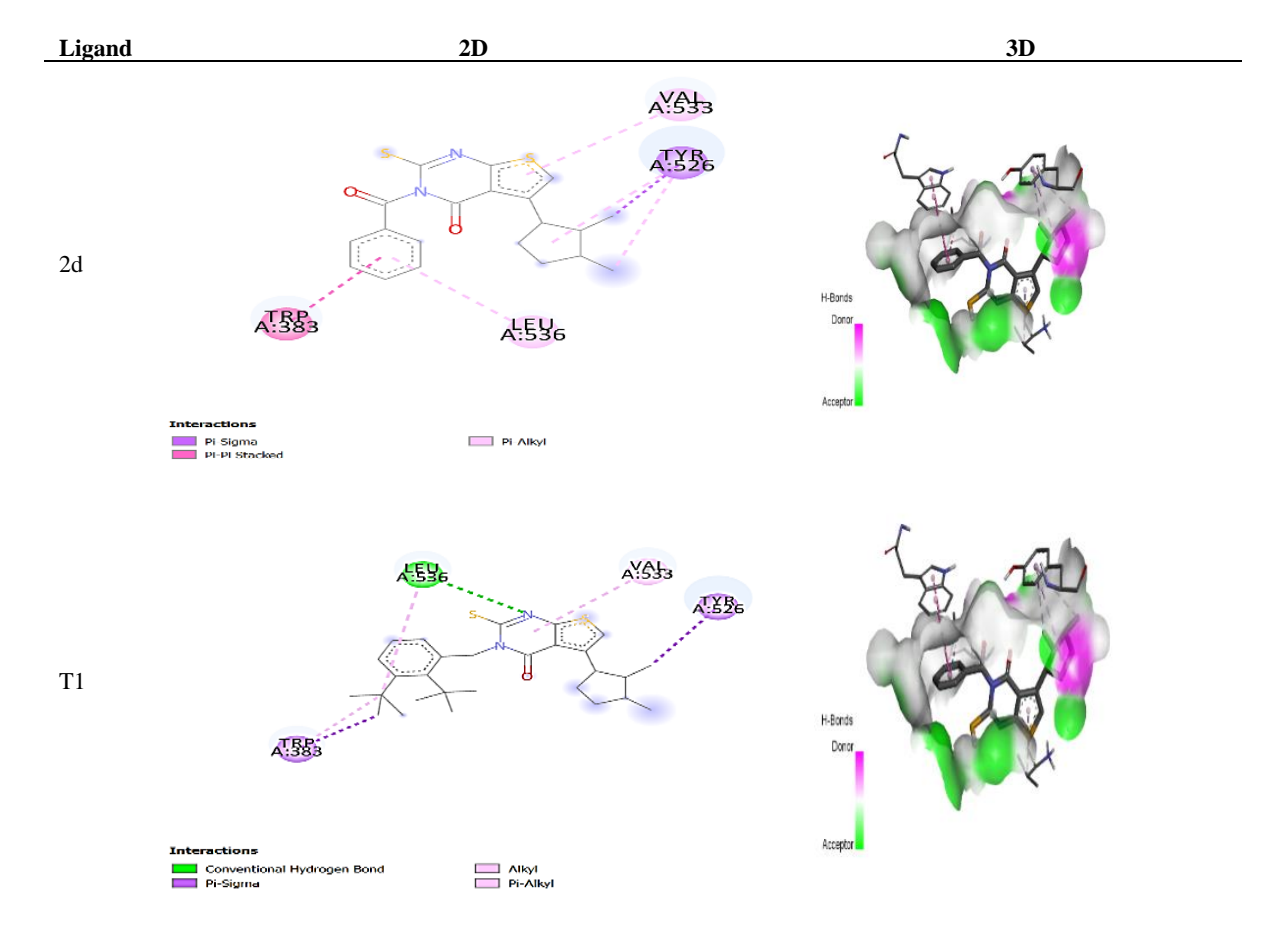
studied compounds interact with amino acids in the same pocket of the receptor's (PDB code 1SJ0) active site. Also, all the proposed compounds have a significant binding affinity.

Table 7. Different interactions between designed molecules and the receptor (ER α) (PDB code 1SJ0).

Designed molecules	Binding affinity [kcal/mol]	Conventional hydrogen bonding	Carbon Hydrogen	Charge attractive	Pi- Anion	Alkyl or Pi-alkyl	Pi-sigma	Pi-sulfur or Pi-stacked
T1	-6.6	Leu 536	None	None	None	Val A:533	Trp A:383	None
T2	-6.3	None	None	None	None	Val A:533 Ala A:350 Trp A:383 Leu A:354 Leu A:536	None	Tyr A:526
T4	-7.2	None	None	None	None	Leu A:354 Leu A:536	Trp A:383 Tyr A:526	Cys A:530
T5	-6.7	None	Cys 530	None	None	Leu A:354 Ala A:350 Trp A:383 Leu A:536	Tyr A:526	Tyr A:530
T6	-7.8	None	None	Asp 351	Asp 351	Leu A:354 Leu A:536 Leu A:525 Ala A:350	Trp A:383	None
2d	-7.4	None	None	None	None	Val A:533 Leu A:536	Trp A:383	Trp A:383

The affinity of the proposed compound and the active molecule of the (ERα) receptor ranged from -7.8 to -6.3 kcal/mol (Table 7). Compounds T1, T2, T4, T5, and T6 showed higher PIC50 activity than the active molecule 2d. Discovery Studio software elucidated the hydrogen and hydrophobic interactions between compounds T1, T2, T4, T5, and T6 and the more active molecule 2d. Compound 32 did not form any hydrogen bonds but demonstrated pisigma and pi-alkyl interactions with the (Me) groups and the residues Val (Valine, A533) and Leu (Leucine, A536). The limited number of bonds reduces the stability of this complex. In contrast, compound T1 established a hydrogen bond with the amine groups via the residues Leu

(Leucine, A536), significantly enhancing the stability of the complex. Additionally, T1 formed two pi-sigma bonding interactions with the residues Trp (Tryptophan, A383) and Tyr (Tyrosine, A526). These important pisigma interactions contribute to a compact structure, with a lower binding affinity than the more active molecule. The proposed molecule T1 exhibits greater potency as an (ERα) receptor inhibitor than the 2d molecule due to its improved binding affinity and interaction stability. The other complexes (T2, T4, T5, and T6) show fewer hydrogen bonds and less effective interactions, making them less stable than T1. This demonstrates that T1 is the most stable complex among those analyzed.



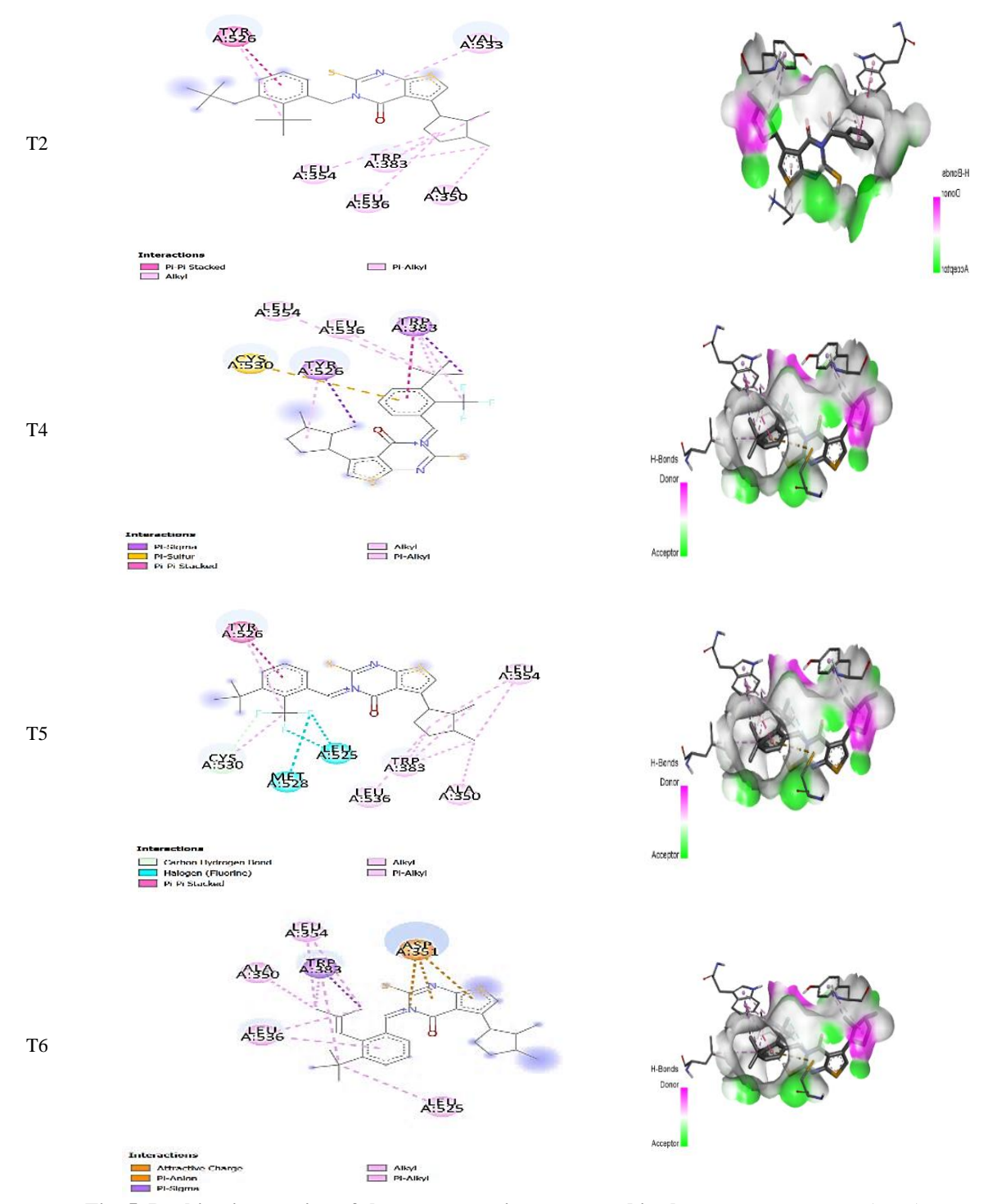


Fig. 5. Docking interaction of the representative compound in the estrogen receptor (ER α)

3.6. Molecular dynamics (MD) simulation of the stability of protein-ligand interactions

A one-hundred-nanosecond simulation using molecular dynamics (MD) was performed to assess the stability of the T1 and 2D complexes formed by the protein **1SJ0** and its associated ligands. Throughout the simulation, according to the trajectory analysis, every ligand maintained its link with the protein's gorge of liaison. Numerous parameters, including the RMSD, RMSF, gyration radius, hydrogen bonding, the average distance between the protein and ligand centers of mass (COM), and free energy of liaison (MMPBSA), have been computed to assess each structure's stability [50].

After the first ten simulation runs, the results showed very little variation, with the RMSD and RMSF values indicating the stability of the complexes [51]. The small variations observed in the radius of gyration suggest that

the stability and compactness of the protein-ligand system are maintained. Throughout the simulation, the hydrogen bonds between the ligands and the protein persisted, and the COM's distance suggested strong stability, especially for ligand T1.

The free energy of binding (ΔG_{Bind}) obtained using the MM-PBSA method was -165.832 \pm 20.069 kJ mol⁻¹ for T1 and -135.295 \pm 15.421 kJ mol⁻¹ for 2D, confirming the strong affinity of the two ligands for the protein. The MM-PBSA calculations also provided the potential energy and the polar and non-polar energy of solvation, highlighting the stability of the interactions in the T1 and 2D complexes [52].

In summary, the simulations have shown the stability and robustness of protein-ligand complexes, offering vital information to comprehend their interaction and potential as therapeutic targets.

Table 8. Calculated binding free energies of the tested compounds [kJ/mol].

		ΔE _{MM} (k	J mol ⁻¹)	ΔG _{Sol} (kJ mol- ¹)		
Complex (Protein- ligand)	ΔG	Van der Waal energy	Electrostatic energy	Polar solvation energy	SASA energy	
T1	-165.832+/-20.069	-194.756+/-16.084	-35.240+/-15.455	86.265+/- 5.823	-22.102+/-1.188	
2D	-135.295+/-15.421	-147.225+/-10.945	-48.464+/-11.157	75.789+/- 9.759	-15.395+/- 1.469	

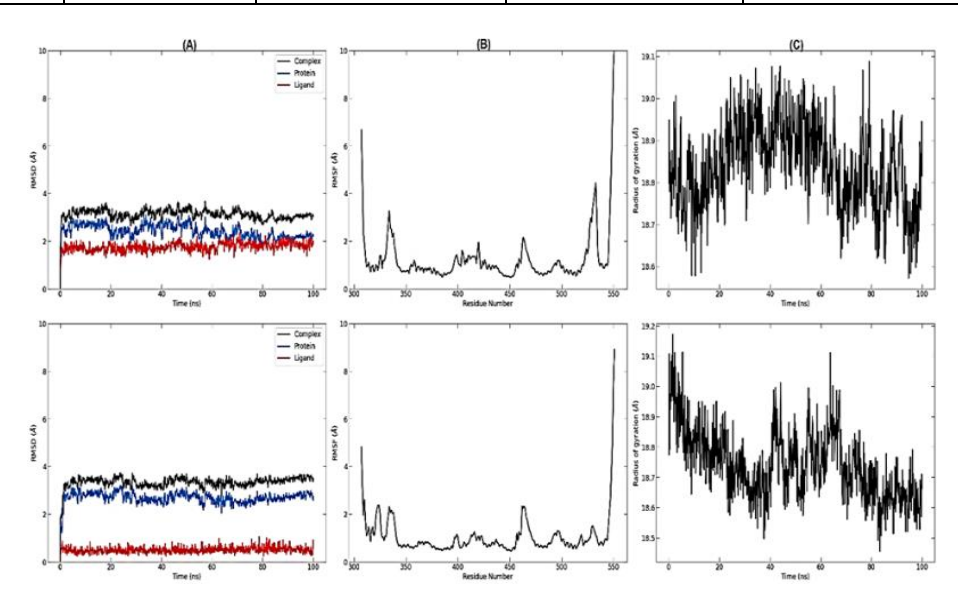


Fig. 6. (A) RMSD, (B) RMSF, and (C) gyratory radius, observed during 100ns MD simulation. T1 (top) and 2D (bottom) complexes.

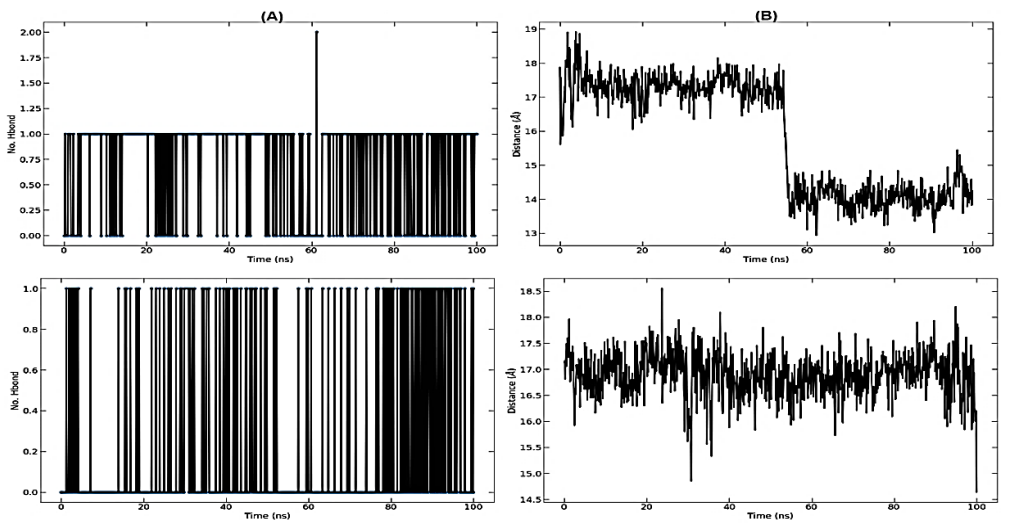


Fig. 7. From right to left: (A) Hydrogen bonds (protein (1SJ0)-ligand (T1 and 2D)) and (B) Average distance between ligand and protein for the complexes during the 100ns MD simulation. Compounds T1 (top) and 2D (bottom)

CONCLUSION

This highlighted study the potential thienopyrimidine inhibitors for the treatment of ER+ breast cancer using advanced computational methods. Through robust 3D-QSAR analyses and molecular docking validation, six new molecules (T1-T6) were identified as promising candidates for estrogen receptor alpha inhibition. The results indicate that these compounds, except T3, which showed mild toxicity, have pharmacokinetic favorable and pharmacodynamic properties and maintain stability within the receptor's active site. Molecular dynamics simulations confirmed their stability, providing valuable insights into the development of new breast cancer drugs. These findings pave the way for future experimental and clinical research to improve therapeutic options for breast cancer patients.

Author Contributions

All participants contributed to the design and

development of the study.

Hassan Badaoui, Youness Moukhliss, Moulay Ahfid Elalaouy, Hanane Zaki, and Marwa Alaqarbeh: creation and design of the research project, data collection, analysis, interpretation of the findings, and article writing; M'barek Choukrad, Hamid Maghat, Abdelouahid Sbai, Mohammed Bouachrine, and Tahar Lakhlifi: revising it critically for important intellectual content, and final approval of the version to be submitted.

Funding: The authors have no outside funding to declare.

Declarations

Conflict of interest: The authors declare no competing interests, as defined by Springer, or other interests that might be perceived to influence the results and/or discussion reported in this paper.

Ethical approval is Not applicable.

REFERENCES

- 1. Antebi A. Nuclear receptor signal transduction in *C. elegans*. In: *WormBook: The Online Review of C. elegans Biology*. WormBook. 2018.
- Jeon S-Y., Hwang K-A., Choi K-C. Effect of steroid hormones, estrogen and progesterone, on epithelial mesenchymal transition in ovarian cancer development. J Steroid Biochem Mol Biol. 2016;158:1–8. https://doi.org/10.1016/j.jsbmb.2016.02.005
- Merrheim J., Villegas J., Van Wassenhove J., Khansa R., Berrih-Aknin S., le Panse R., Dragin N. Estrogen, estrogen-like molecules and autoimmune diseases. *Autoimmun Rev.* 2020;19:102468. https://doi.org/10.1016/j.autrev.2020.102468
- Speltz T.E., Mayne C.G., Fanning S.W., Siddiqui Z., Tajkhorshid E., Greene G.L., Moore T.W. A "Cross-Stitched" Peptide with Improved Helicity and Proteolytic Stability. Org Biomol Chem. 2018;16:3702–6. https://doi.org/10.1039/c8ob00790j
- Hegde M., Girisa S., Naliyadhara N., Kumar A., Alqahtani M.S., Abbas M., Mohan C.D., Warrier S., Hui K.M., Rangappa K.S., Sethi G., Kunnumakkara A.B. Natural compounds targeting nuclear receptors for effective cancer therapy. *Cancer Metastasis Rev.* 2023;42:765–822. https://doi.org/10.1007/s10555-022-10068-w
- 6. Vishnoi K., Viswakarma N., Rana A., Rana B. Transcription Factors in Cancer Development and Therapy. *Cancers* (*Basel*). 2020;12:2296. https://doi.org/10.3390/cancers12082296
- Taheri M., Shoorei H., Dinger M.E., Ghafouri-Fard S. Perspectives on the Role of Non-Coding RNAs in the Regulation of Expression and Function of the Estrogen Receptor. *Cancers* (*Basel*). 2020;12:2162. https://doi.org/10.3390/cancers12082162

- Tetruashvili N., Domar A., Bashiri A. Prevention of Pregnancy Loss: Combining Progestogen Treatment and Psychological Support. *JCM*. 2023;12:1827. https://doi.org/10.3390/jcm12051827
- Ali I., Lone M.N., Aboul-Enein H.Y. Imidazoles as potential anticancer agents †The authors declare no competing interests. *Medchemcomm*. 2017;8:1742–1773. https://doi.org/10.1039/c7md00067g
- George S., Abrahamse H. Redox Potential of Antioxidants in Cancer Progression and Prevention. Antioxidants (Basel). 2020;9:1156. https://doi.org/10.3390/antiox9111156
- 11. Song S., Kim S., El-Sawy E.R., Cerella C., Orlikova-Boyer B., Kirsch G., Christov C., Dicato M., Diederich M. Anti-Leukemic Properties of Aplysinopsin Derivative EE-84 Alone and Combined to BH3 Mimetic A-1210477. *Mar Drugs*. 2021;19:285. https://doi.org/10.3390/md19060285
- Ardevines S., Marqués-López E., Herrera R.P. Heterocycles in Breast Cancer Treatment: The Use of Pyrazole Derivatives. *Curr Med Chem.* 2023;30:1145– 1174.
 - https://doi.org/10.2174/0929867329666220829091830
- Kolawole O.A., Banjo S. In Vitro Biological Estimation of 1,2,3-Triazolo[4,5-d]pyrimidine Derivatives as Antibreast Cancer Agent: DFT, QSAR and Docking Studies. *Curr Pharm Biotechnol*. 2020;21:70–78. https://doi.org/10.2174/1389201020666190904163003
- 14. Thapa R., Flores R., Cheng K.H., Mochona B., Sikazwe D. Design and Synthesis of New Acyl Urea Analogs as Potential σ1R Ligands. *Molecules*. 2023;28:2319. https://doi.org/10.3390/molecules28052319

- 15. Aati H.Y., Attia H., Babtin R., Al-Qahtani N., Wanner J. Headspace solid phase micro-extraction of volatile constituents produced from Saudi *Ruta chalepensis* and molecular docking study of potential antioxidant activity. *Molecules*. 2023;28:1891.
 - https://doi.org/10.3390/molecules28041891
- 16. Frant M.P., Trytek M., Deryło K., Kutyła M., Paduch R. Cellular localization of selected porphyrins and their effect on the in vitro motility of human colon tumors and normal cells. *Molecules*. 2023;28:2907. https://doi.org/10.3390/molecules28072907
- 17. [Author(s) missing] Antimicrobial, antibiofilm, and anticancer activities of *Syzygium aromaticum* essential oil nanoemulsion. *PMC*. [n.d.] https://www.ncbi.nlm.nih.gov/pmc/articles/PMC104212 52/
- Maimaitiming M., Lv L., Zhang X., Xia S., Li X., Wang P., Liu Z., Wang C.-Y. Semi-synthesis and biological evaluation of 25(R)-26-acetoxy-3β,5α-dihydroxycholest-6-one. *Mar Drugs*. 2023;21:191. https://doi.org/10.3390/md21030191
- Thiriveedhi A., Nadh R.V., Srinivasu N., Bobde Y., Ghosh B., Sekhar K.V.G.C. Design, synthesis and antitumour activity of new pyrimidine-pyrrole appended triazoles. *Toxicol In Vitro*. 2019;60:87–96. https://doi.org/10.1016/j.tiv.2019.05.009
- 20. Kis B., Moacă E.-A., Tudoran L.B., Muntean D., Magyari-Pavel I.Z., Minda D.I., Lombrea A., Diaconeasa Z., Dehelean C.A., Dinu Ş., Danciu C. Green synthesis of silver nanoparticles using *Populi gemmae* extract: Preparation, physicochemical characterization, antimicrobial potential and in vitro antiproliferative assessment. *Materials* (*Basel*). 2022;15:5006. https://doi.org/10.3390/ma15145006

- 21. El-Sharkawy K.A., Bratty M.A., Alhazmi H.A., Najmi A. Design, synthesis, and biological activities of novel thiophene, pyrimidine, pyrazole, pyridine, coumarin and isoxazole: Dydrogesterone derivatives as antitumor agents. *Open Chemistry*. 2021;19:322–337. https://doi.org/10.1515/chem-2021-0028
- 22. Wilkes J.G., Stoyanova-Slavova I.B., Buzatu D.A. Alignment-independent technique for 3D QSAR analysis. J Comput Aided Mol Des. 2016;30:331–345. https://doi.org/10.1007/s10822-016-9909-0
- 23. Pan M., Cheng L., Wang Y., Lyu C., Hou C., Zhang Q. Exploration of 2D and 3D-QSAR analysis and docking studies for novel dihydropteridone derivatives as promising therapeutic agents targeting glioblastoma. *Front Pharmacol.* 2023;14:1249041. https://doi.org/10.3389/fphar.2023.1249041
- 24. Er-Rajy M., El Fadili M., Imtara H., Saeed A., Ur Rehman A., Zarougui S., Abdullah S.A., Alahdab A., Parvez M.K., Elhallaoui M. 3D-QSAR Studies, Molecular Docking, Molecular Dynamic Simulation, and ADMET Proprieties of Novel Pteridinone Derivatives as PLK1 Inhibitors for the Treatment of Prostate Cancer. *Life (Basel)*. 2023;13:127. https://doi.org/10.3390/life13010127
- 25. Aouidate A., Ghaleb A., Ghamali M., Chtita S., Ousaa A., Choukrad M., Sbai A., Bouachrine M., Lakhlifi T. Computer aided drug design based on 3D-QSAR and molecular docking studies of 5-(1H-indol-5-yl)-1,3,4-thiadiazol-2-amine derivatives as PIM2 inhibitors: a proposal to chemists. *In Silico Pharmacol.* 2018;6:5. https://doi.org/10.1007/s40203-018-0043-7
- 26. Daina A., Michielin O., Zoete V. SwissADME: a free web tool to evaluate pharmacokinetics, drug-likeness and medicinal chemistry friendliness of small molecules. *Sci Rep.* 2017;7:42717. https://doi.org/10.1038/srep42717
- 27. Benet L.Z., Hosey C.M., Ursu O., Oprea T.I. BDDCS, the Rule of 5 and Drugability. *Adv Drug Deliv Rev*. 2016;101:89–98. https://doi.org/10.1016/j.addr.2016.05.007

- 28. O'Shea J.P., Augustijns P., Brandl M., Brayden D.J., Brouwers J., Griffin B.T., Holm R., Jacobsen A.-C., Lennernäs H., Vinarov Z., O'Driscoll C.M. Best practices in current models mimicking drug permeability in the gastrointestinal tract - An UNGAP review. *European Journal of Pharmaceutical Sciences*. 2022;170:106098. https://doi.org/10.1016/j.ejps.2021.106098
- Durán-Iturbide N.A., Díaz-Eufracio B.I., Medina-Franco J.L. In Silico ADME/Tox Profiling of Natural Products: A Focus on BIOFACQUIM. ACS Omega. 2020;5:16076– 16084. https://doi.org/10.1021/acsomega.0c01581
- Sharma D., Kumar S., Narasimhan B. Estrogen alpha receptor antagonists for the treatment of breast cancer: a review. *Chem Cent J.* 2018;12:107.
 - $\underline{https://doi.org/10.1186/s13065\text{-}018\text{-}0472\text{-}8}$
- Trott O., Olson A.J. AutoDock Vina: improving the speed and accuracy of docking with a new scoring function, efficient optimization, and multithreading. *J Comput Chem.* 2010;31:455–461.
 - https://doi.org/10.1002/jcc.21334
- 32. Bank R.P.D. RCSB PDB 1SJ0: Human Estrogen Receptor Alpha Ligand-binding Domain in Complex with the Antagonist Ligand 4-D. RCSB Protein Data Bank. [Online] Available from:
 - https://www.rcsb.org/structure/1sj0
- Kumar R., Zakharov M.N., Khan S.H., Miki R., Jang H., Toraldo G., Singh R., Bhasin S., Jasuja R. The Dynamic Structure of the Estrogen Receptor. *J Amino Acids*. 2011;2011:812540. https://doi.org/10.4061/2011/812540
- 34. Fu Y., Zhao J., Chen Z. Insights into the Molecular Mechanisms of Protein-Ligand Interactions by Molecular Docking and Molecular Dynamics Simulation: A Case of Oligopeptide Binding Protein. *Comput Math Methods Med.* 2018;2018:3502514.
 - https://doi.org/10.1155/2018/3502514

- 35. Kognole A.A., Lee J., Park S.-J., Jo S., Chatterjee P., Lemkul J.A., Huang J., MacKerell A.D., Im W. CHARMM-GUI Drude prepper for molecular dynamics simulation using the classical Drude polarizable force field. *J Comput Chem.* 2022;43:359–375. https://doi.org/10.1002/jcc.26795
- 36. Kim S., Lee J., Jo S., Brooks C.L., Lee H.S., Im W. CHARMM-GUI Ligand Reader & Modeler for CHARMM Force Field Generation of Small Molecules. *J Comput Chem.* 2017;38:1879–1886. https://doi.org/10.1002/jcc.24829
- 37. Alencar W.L.M., da Silva Arouche T., Neto A.F.G., de Castro Ramalho T., de Carvalho Júnior R.N., de Jesus Chaves Neto A.M. Publisher Correction: Interactions of Co, Cu, and non-metal phthalocyanines with external structures of SARS-CoV-2 using docking and molecular dynamics. *Sci Rep.* 2022;12:4326. https://doi.org/10.1038/s41598-022-08312-y
- 38. Lee J., Cheng X., Swails J.M., Yeom M.S., Eastman P.K., Lemkul J.A., Wei S., Buckner J., Jeong J.C., Qi Y., Jo S., Pande V.S., Case D.A., Brooks C.L., MacKerell A.D., Klauda J.B., Im W. CHARMM-GUI Input Generator for NAMD, GROMACS, AMBER, OpenMM, and CHARMM/OpenMM Simulations Using the CHARMM36 Additive Force Field. *J Chem Theory Comput.* 2016;12:405–413.
 - https://doi.org/10.1021/acs.jctc.5b00935
- 39. Pereira G.R.C., Abrahim-Vieira B. de A., de Mesquita J.F. In Silico Analyses of a Promising Drug Candidate for the Treatment of Amyotrophic Lateral Sclerosis Targeting Superoxide Dismutase I Protein. *Pharmaceutics*. 2023;15:1095.
 - https://doi.org/10.3390/pharmaceutics15041095
- Kumari R., Kumar R., Open Source Drug Discovery Consortium, Lynn A. g_mmpbsa--a GROMACS tool for high-throughput MM-PBSA calculations. *J Chem Inf Model*. 2014;54:1951–1962.
 - https://doi.org/10.1021/ci500020m

- Gundelach L., Fox T., Tautermann S.T., Skylaris C.-K. Protein-ligand free energies of binding from full-protein DFT calculations: convergence and choice of exchange-correlation functional. *Physical Chemistry Chemical Physics*. 2021; 23:9381–9393.
- 42. In silico studies of a novel scaffold of benzoxazole derivatives as anticancer agents by 3D-QSAR, molecular docking and molecular dynamics simulations. *RSC Advances*. 2023; DOI:10.1039/D3RA01316B.
- 43. Pandey P.K., Sharma A.K., Gupta U. Blood brain barrier: An overview on strategies in drug delivery, realistic in vitro modeling and in vivo live tracking. *Tissue Barriers*. 2016; 4:e1129476.
- 44. Wu Q., Yan R., Sun J. Probing the drug delivery strategies in ischemic stroke therapy. *Drug Delivery*, 2020; 27:1644–1655.
- 45. Iacopetta D., Ceramella J., Catalano A., Scali E., Scumaci D., Pellegrino M., Aquaro S., Saturnino C., Sinicropi M.S. Impact of Cytochrome P450 Enzymes on the Phase I Metabolism of Drugs. Applied Sciences. 2023; 13:6045.
- 46. Miners J.O., Birkett D.J. Cytochrome P4502C9: an enzyme of major importance in human drug metabolism. British Journal of Clinical Pharmacology. 1998; 45:525–538Jarvis, J.P., Peter, A.P., Shaman, J.A.: Consequences of CYP2D6 Copy-Number Variation for Pharmacogenomics in Psychiatry. Frontiers in Psychiatry. 10, (2019)

- 47. Sarkar P., Alheety M.A., Srivastava V. Molecular docking and ADMET study of spice-derived potential phytochemicals against human DNA topoisomerase III alpha. *Macromolecular Symposia*. 2023; 407:2200108.
- 48. Samiei M., Asgary S., Farajzadeh M., Bargahi N., Abdolrahimi M., Kananizadeh U., Dastmalchi S. Investigating the mutagenic effects of three commonly used pulpotomy agents using the Ames test. *Advanced Pharmaceutical Bulletin*. 2015; 5:121–125.
- 49. Al-Shaar M., Mando H., Alkhatib R. In silico antioxidant activity of six volatile constituents in Capsella bursa-pastoris. Jordan Journal of Pharmaceutical Sciences. 2025; 18(1):230–244.
- 50. Maslov O., Komisarenko M., Kolisnyk S., Derymedvid L. Evaluation of anti-inflammatory, antioxidant activities and molecular docking analysis of *Rubus idaeus* leaf extract. *Jordan Journal of Pharmaceutical Sciences*. 2024; 17(1):105–122.
- 51. Msafer B.A.A., Abbas M.A., Shaer W.A., Arafat S. Enhanced platelet activation induced by palbociclib treatment in MCF-7 breast cancer cells. *Jordan Journal of Pharmaceutical Sciences*. 2025; 18(1):10–20.

دراسة حوسبية متكاملة لمشتقات بنزويل ثينوبيريميدين كمنظمات محتملة لمستقبل الإستروجين ${ m Er}\alpha$ في علاج سرطان الثدى

حسن بداوي1، مروه العقاربه 2°، يونس مخلص1، حنان زكي3، مولاي أحفيظ العلوي1، مبارك شوكراد1، عبد الواحد السباعي1، حميد معالي مخات1، الطاهر الأخليفي1، محمد بوعشربن1

ملخص

يعد سرطان الثدي المعتمد على الهرمونات والموجب لمستقبلات الإستروجين (+ER) هو النوع الأكثر شيوعًا لدى النساء حيث يمثل حوالي 75% من جميع الحالات. تهدف هذه الدراسة إلى اقتراح عوامل علاجية جديدة محتملة لسرطان الثدي باستخدام الطرق الحوسبية تم إجراء دراسة ثلاثية الأبعاد للعلاقة الكمية بين البنية والنشاط (3 (COMSAR) مركبًا مستندة إلى أبحاث سابقة، وقد أظهرت قدرة تنبؤية قوية كما يتضح من القيم العالية لـ COMSIA0 و COMSIA1 لطريقتي CoMSIA1 و Comsia2 من القراح ست جزيئات جديدة (Comsia3 بهدف تعزيز النشاط المثبط، وقد أظهرت نتائج تحليل الارتباط الجزيئي أن الجزيئات المرشحة أحرزت نتائج مميزة واستقرت في موقع الارتباط داخل المستقبل رمز (Comsia4 كما أظهرت المركبات المقترحة خصائص دوائية وحركية حيوية مناسبة، باستثناء Comsia4 الذي أظهر سمية خفيفة. وأكدت محاكاة الديناميكيات الجزيئية أن المعقدين Comsia4 مستقران في الموقع الفعال لمستقبل الإستروجين Comsia5 تسلط هذه النتائج الضوء على إمكانيات المركبات المبنية على الثينوبيريميدين كمضادات محتملة لسرطان الثدي، مما يفتح آفاقًا جديدة للبحث التجريبي والسريري.

الكلمات الدالة: سرطان الثدي، النمذجة الحوسبية، الامتصاص والتوزيع والتمثيل والإخراج/السمّية،الثينوبيريميدين، العلاقة الكمية ثلاثية الأبعاد بين البنية والنشاط.

تاريخ استلام البحث 2024/6/17 وتاريخ قبوله للنشر 2024/9/21.

¹ مختبر الكيمياء الجزيئية والمواد الطبيعية، كلية العلوم، جامعة مولاي إسماعيل بمكناس، المغرب

² أكاديمية الأمير حمين بن عبدالله الثاني للحماية المدنية، جامعة البلقاء التطبيقية، السلط، الأردن

³ مختبر التكنولوجيا الحيوية والموارد البيولوجية والمعلوماتية الحيوية، المدرسة العليا للتكنولوجيا، جامعة السلطان3 مولاي سليمان، خنيفرة، المغرب

^{*} المؤلف المراسل: مروه العقاربه

marwaqabh@hotmail.com; marwa.aqarbeh@bau.edu.jo